# Computational Investigation of Irreversible Inactivation of the Zinc-Dependent Protease Carboxypeptidase A

**Jason B. Cross,[†,#] Thom Vreven,[‡] Samy O. Meroueh,[§] Shahriar Mobashery,[§] and H. Bernhard Schlegel*,[†]**

*Department of Chemistry, Wayne State University, Detroit, Michigan 48202, Gaussian, Inc., 340 Quinnipiac Street, Bldg 40, Wallingford, Connecticut 06492, and Department of Chemistry and Biochemistry, University of Notre Dame, Notre Dame, Indiana 46556*

Zinc proteases are ubiquitous and the zinc ion plays a central function in the catalytic mechanism of these enzymes. A novel class of mechanism-based inhibitors takes advantage of the zinc ion chemistry in carboxypeptidase A (CPA) to promote covalent attachment of an inhibitor to the carboxylate of Glu-270, resulting in irreversible inhibition of the enzyme. The effect of the active site zinc ion on irreversible inactivation of CPA was probed by molecular orbital (MO) calculations on a series of active site models and the $Cl^-$ + $CH_3Cl$ $S_N2$ reaction fragment. Point charge models representing the active site reproduced energetics from full MO calculations at 12.0 Å separation between the zinc and the central carbon of the $S_N2$ reaction, but at 5.0 Å polarization played an important role in moderating barrier suppression. ONIOM MO/MO calculations that included the residues within 10 Å of the active site zinc suggest that about 75% of the barrier suppression arises from the zinc ion and its ligands. A model of the pre-reactive complex of the 2-benzyl-3-iodopropanoate inactivator with CPA was constructed from the X-ray structure of L-phenyl lactate bound in the active site of the enzyme. The model was fully solvated and minimized by using the AMBER force field to generate the starting structure for the ONIOM QM/MM calculations. Optimization of this structure led to the barrierless $S_N2$ displacement of the iodide of the inhibitor by Glu-270, assisted by interaction of the zinc ion with the leaving group. The resulting product is in good agreement with the X-ray structure of the covalently modified enzyme obtained by irreversible inhibition of CPA by 2-benzyl-3-iodopropanoate.

## Introduction

Transition metals bind to enzymes for both structural and mechanistic reasons. As many as a quarter of the known enzymes contain metals in their active sites. In essence, the metal ion expands the repertoire of the reactions that enzymes can perform by either providing redox capacity or acting as Lewis acids. The mechanistic influences metals can have on the catalytic processes of enzymes are beginning to be understood by using a combination of experimental methods and electronic structure calculations.

One of the most common transition metals found in enzymes is the zinc ion. A novel set of enzyme inactivators that takes advantage of the chemistry of the zinc ion in the active site of the zinc-dependent protease carboxypeptidase A (CPA) in its inactivation chemistry has been described.[1−4] In one strategy, we demonstrated that coordination of an unactivated alkyl halide with the active site zinc ion in CPA promoted displacement of the halide ion by a glutamate carboxylate by several orders of magnitude (Figure 1).[3,4] This covalent modification of the enzyme in the active site led to irreversible inactivation, or suicide inhibition,[5] of CPA.[3,4]

Given the difficulty of probing these types of reactions experimentally, it is advantageous to use theoretical methods to investigate such processes. Molecular orbital (MO) methods can be used to generate an accurate description of relative energies and geometries on a reaction path. However, computational bottlenecks arise when attempting to treat systems the size of enzymes. Early theoretical studies of zinc enzymes focused on binding and reactivity of small molecules in the first coordination sphere of the $Zn^{2+}$ ion.[6−9] Other studies added a small portion of the active site environment by including the side chains of amino acid residues bonded to the $Zn^{2+}$ ion and holding these residues in their relative positions in the active site.[10−12] More accurate models included structural elements of the protein that kept the active site residues properly aligned,[13] as well as electrostatic interactions that may have played a role in the catalysis. In a recent paper by Siegbahn and co-workers, the mechanism of substrate turnover by thermolysin, an enzyme that is structurally related to CPA, was studied using density functional theory.[14] The computed reaction path contained a Zn-bound water in the reactant structure and had a calculated activation energy of 15.2 kcal/mol, which was comparable to the 12.4−16.3 kcal/mol observed experimentally.[14,15] A number of mechanistic issues regarding zinc metalloenzymes were resolved in this study and a mechanism for thermolysin was proposed that contained elements of both commonly proposed mechanisms for zinc enzymes: the zinc−carbonyl mechanism, in which the substrate binds directly to zinc, and the zinc−hydroxide mechanism, in which zinc functions through a catalytic water molecule.[14]

In this report, we have used QM/MM calculations to investigate the irreversible inactivation of CPA by 2-benzyl-3-

* Address correspondence to this author. E-mail: hbs@chem.wayne.edu.
† Wayne State University.
# Current address: Affinium Pharmaceuticals, 100 University Avenue, 12th Floor, North Tower, Toronto, Ontario M5J 1V6.
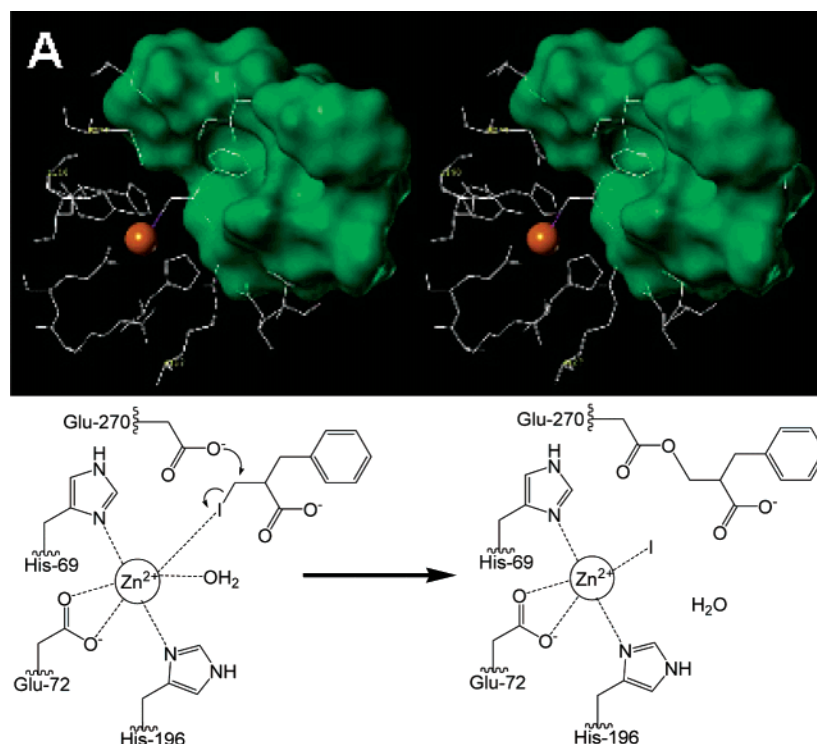‡ Gaussian, Inc.
§ University of Notre Dame.

**Figure 1.** (A) Stereo image of the energy-minimized complex of 2-benzyl-3-iodopropanoate bound to the active site of CPA. The hydrophobic binding pocket for the benzyl group is depicted as a Connolly surface (green). (B) A schematic of the interactions of the inhibitor in the active site and the metal-ion-facilitated reaction that leads to covalent modification of Glu-270. Covalent modification of Glu-270 was documented by X-ray analysis of the inactivated enzyme (ref 4).

iodopropanoate. QM/MM methods employ the strengths of both MO and classical force field calculations and have been used successfully on a number of biological systems.[16−25] By treating the active site region with high-level MO theory and the more distant parts of the protein with a classical force field, accurate calculations can be performed on systems containing thousands of atoms. The inactivation of CPA by 2-benzyl-3-iodopropanoate occurs via an $S_N2$ reaction with Glu-270 and is thought to be facilitated by the electrostatic effects of the zinc ion. Recent work has suggested that similar electrostatic effects may be dominant factors in many enzymatic reactions[26,27] and related studies have shown that such catalysis can also occur in uniform media by introducing an electric field.[28,29] To obtain preliminary data on the influence of electrostatics on the inactivation reaction, we have probed models of the active site of CPA with a very simple $S_N2$ reaction. We then employed the ONIOM QM/MM method with electronic embedding[30−32] to study the actual inhibitor in the full enzyme.

**Computational Methods**

Molecular orbital (MO) calculations were carried out using the GAUSSIAN 03 series of programs.[33] The structures of CPA, and CPA with L-phenyl lactate and 2-benzyl-3-iodopropanoate inhibitors were obtained from the Research Collaboratory for Structural Bioinformatics database (http://www.rcsb.org/pdb/index.html) with accession numbers 2CTB, 2CTC, and 1BAV, respectively. The X-ray coordinates of 2CTB were used to generate the active site models of CPA. MO calculations and geometry optimizations of complexes and transition states using active site models were computed by quantum mechanical calculations and by QM/QM and QM/MM calculations. Unless otherwise indicated, Mulliken population analysis was used as a simple probe of the charge distribution and electrostatic interactions. For the smaller active site calculations, the Har-

tree−Fock method[34] with the 6-31G(d) basis set[35,36] was used, since it is known to be satisfactory for simple $S_N2$ reactions such as $Cl^- + CH_3Cl$ in the gas phase.[37] Density functional calculations generally underestimate the central barrier height of $S_N2$ reactions. MP2 and higher level results agree well with the Hartree−Fock calculations but would be too costly for the larger models of the active site. The Wachters−Hay basis set[38−40] provides a reliable description for transition metals and was used for the active site zinc ion. Ab initio molecular orbital calculations become computationally very expensive as the size of the system increases. For larger active site models, we employed a multilayer ab initio/semiempirical QM/QM approach, carried out with the ONIOM method.[30−32] This allowed the small, reactive part of the enzyme active site to be treated using ab initio methods, while the spectator residues surrounding the active site were treated by a less expensive semiempirical method. In this way, more of the enzyme could be included in the calculations and long-range effects that are normally left out of limited ab initio calculations, such as those due to electrostatic interactions with the surrounding residues, were taken into account. For the single point calculations with the ONIOM method, the ab initio layer was calculated using Hartree−Fock theory and the basis set described above, while the semiempirical layer was calculated using AM1.[41] This model included approximately 350 atoms and 1000 basis functions.

For the full enzyme−inhibitor complex, mixed quantum/classical (QM/MM) calculations were carried out with a two-layer ONIOM method[30−32] using electronic embedding.[42] The enzyme was divided into a high-level layer, which was treated at the HF/6-31G(d) level of theory, and a low-level layer, which was treated with the AMBER force-field using the "parm96" set of parameters.[43] Electronic embedding allows the wave function of the quantum layer to be influenced by the electrostatic field of the classical layer using the partial charges defined

in AMBER. Because of a lack of parameters for zinc, the active site Zn in the AMBER calculations (both in the real and the model system) is replaced by Li, for which there are parameters. Because a difference is taken, $E_{MM}^{Real} - E_{MM}^{Model}$, these terms cancel completely and only the QM calculations contribute to the interaction between Zn, its ligands, and the active site. Furthermore, the two chlorides are treated as isolated atoms in the MM calculations so that the bond elongation does not cause any numerical problems. A number of covalent bonds cross the interface between the QM and MM layers, both in the residues coordinated to the zinc ion and in the nonreactive portion of the 2-benzyl-3-iodopropanoate inhibitor. Special consideration was required for these regions, since large molecular mechanics (MM) charges close to the quantum mechanical (QM) region may cause overpolarization of the wave function. This was overcome by scaling the MM charges close to the interface region.[32] Link atoms added to the model system were assigned a charge of zero. The majority of the protein was held fixed in Cartesian space, allowing only 73 atoms within the active site region to move during geometry optimization. This reduced the numerical noise in the relative energies due to conformational changes distant from the active site.

Additional steps were required to prepare the enzyme structure for QM/MM calculations. Manipulation of the 2CTC X-ray structure was carried out using SYBYL 6.7.[44] This included modification of the ligand present in the X-ray structure (L-phenyl lactate) to the structurally similar 2-benzyl-3-iodopropanoate. Hydrogen atoms were added to the enzyme structure using the program Protonate, which is a part of the AMBER 6 suite of programs.[45] Force-field parameters and atomic charges for protein residues were obtained from the "parm99" set of parameters.[46] Atomic charges of the 2-benzyl-3-iodopropanoate inhibitor were computed using the RESP fitting procedure[47] and are listed in the Supporting Information. The protein was placed in a box of TIP3P water with at least 10 Å between any face of the box and the enzyme. The solvated enzyme system consisted of 52 760 atoms. Water molecules were equilibrated by running a 40 ps MD simulation while holding the protein fixed. This was followed by 20 000 steps of conjugate-gradient energy minimization of the entire system. The resulting structure, which included a layer of all water molecules within 3.0 Å of the enzyme, was used as a starting point for QM/MM calculations.

## Results and Discussion

As shown in Figure 1, we have previously reported a novel class of inhibitors for the zinc-dependent protease, CPA. The inhibitor was designed to bind to the active site of this enzyme, bringing an unactivated halide to the coordination sphere of the zinc ion. We demonstrated that the coordinated halide was displaced nucleophilically by Glu-270, a critical residue for the catalytic mechanism of the enzyme.[4] Covalent modification of the glutamate by the inhibitor resulted in irreversible inactivation of the enzyme. We demonstrated that the rate constant for this reaction, which takes place in the confines of the active site, was enhanced by several orders of magnitude over the corresponding nonenzymatic reaction.[3] Clearly, the zinc ion and the protein environment within the active site of the enzyme played key roles. This type of metal activation in the displacement of halogens is well precedented in organic synthesis.[48−54]

To probe the electrostatic effect of the active site of CPA on reaction of the suicide inhibitor with Glu-270, we first examined a series of simple models. The generic $S_N2$ reaction of Cl⁻ with CH₃Cl has been well studied both experimentally and theoretically.[55−59] Changes in the energetics of this model

reaction were examined as the components of the active site were added. These model calculations served as a probe for the events and interactions in the active site of CPA during inactivation. QM/MM calculations were then used to compute the covalent attachment of the irreversible inhibitor, 2-benzyl-3-iodopropanoate, to Glu-270 in the full enzyme.

**Preliminary Calculations on Model Systems.** *Model A.* The simplest model of the metalloenzyme that can be used to test the effects of the electrostatic environment on a nucleophilic displacement reaction is to use a suitably placed point charge (or ion) and a generic $S_N2$ reaction. Model A, shown in Figure 2, consisted of the Cl⁻ + CH₃Cl reaction with the zinc ion constrained to lie along the reaction coordinate. Isolated in the gas phase, CH₃Cl and Cl⁻ form a tightly bound ion−molecule complex. At the HF/6-31G(d) level of theory, the barrier from this complex to the transition state is 13.9 kcal/mol,[37] which compares favorably with experimental estimates of 11.6 ± 1.8 kcal/mol.[37,60] The zinc ion was placed at a number of fixed distances from the central carbon and the geometries of the ion−molecule complex and transition state were re-optimized. The reaction barrier disappeared when the zinc ion was 10 Å or less from the central carbon in the $S_N2$ reaction. At shorter distances there was considerable charge transfer, leaving the chlorine neutral and zinc with a +1 charge. To check the behavior in the absence of charge transfer, the zinc ion was replaced with a bare +2 point charge without any basis functions. The barrier also disappeared at distances of 10 Å or less due to the strong electrostatic interactions between the model reaction and the point charge.

*Model B.* Clearly, the effect of a bare zinc ion on the model $S_N2$ reaction was rather extreme. In the active site, the zinc ion is coordinated to His-69, Glu-72, and His-196, which serve to partially neutralize the charge (the charge on the zinc was reduced to +1.32). Model B (Figure 2) consisted of the zinc ion, two imidazoles, and a formate ion, which model the side chains of His-69, His-196, and Glu-72 in the active site. The relative orientations of these side chain fragments were maintained by fixing the Cartesian coordinates of the terminal hydrogen atoms, which replaced the $C_\gamma$ for Glu-72 and $C_\beta$ for both His residues. The zinc ion and the Cl⁻ + CH₃Cl moiety were constrained to be collinear, and the orientation was determined by optimization.

The reaction paths for two cases were studied. In the first case, the distance between the central $S_N2$ carbon in the reaction fragment and the $Zn^{2+}$ ion was held fixed at 12.0 Å. This corresponded to the approximate distance at which the barrier disappeared in Model A, with the departing chloride remaining outside the coordination sphere of the metal ion. In the second case, the separation distance was fixed at 5.0 Å, to permit coordination between the displaced halide and the $Zn^{2+}$ ion. In both cases, the starting point on the reaction path was taken as the geometry of the pre-reactive ion−molecule complex. Several points on the reaction path were obtained by lengthening the $Cl_1-C$ bond in 0.1 Å increments and optimizing the remaining parameters. In addition to providing an energy profile along the reaction path, this provides an approximate location for the transition state. The transition state was then fully optimized without the $Cl_1-C$ bond constraint.

The relative energies of the optimized structures on the 12.0 Å reaction path are plotted in Figure 3A. At this distance the transition state barrier was 8.8 kcal/mol (a barrier suppression of 5.1 kcal/mol or 37% compared to the gas phase reaction). To check whether this barrier suppression was primarily the result of electrostatic effects, single point energies for the
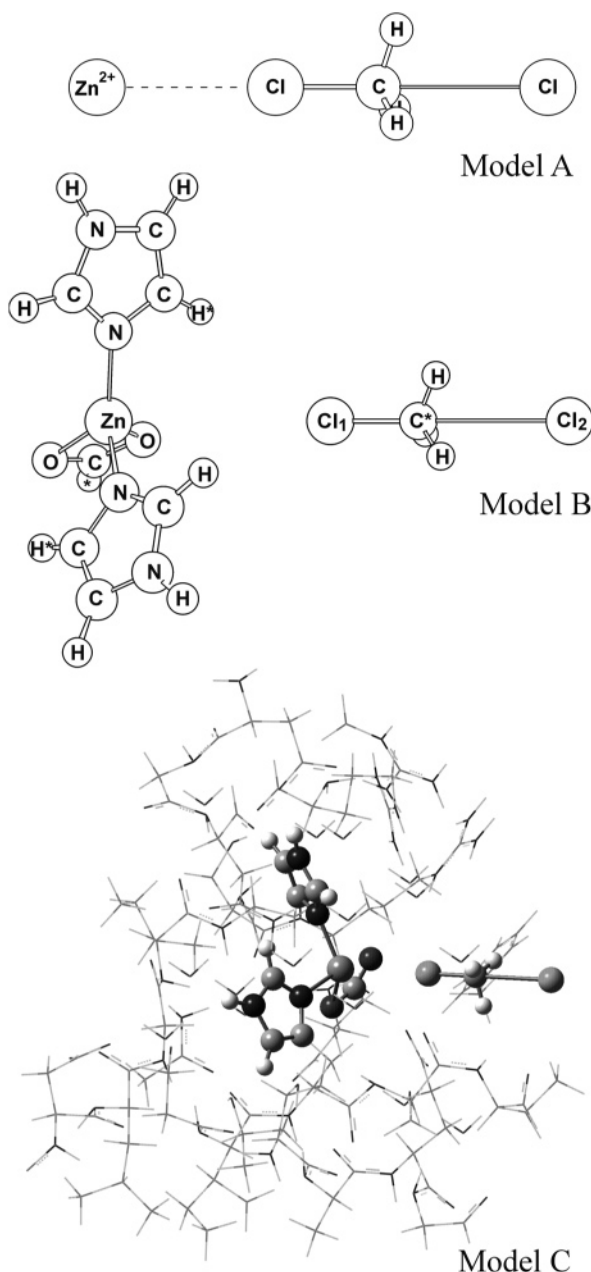
**Figure 2.** Computational models of barrier suppression in a simple $S_N2$ reaction. Model A consisted of the $Cl^- + CH_3Cl$ $S_N2$ reaction with $Zn^{2+}$ placed along the reaction coordinate. Model B included the side chains of His-69, Glu-72, and His-196, the catalytic zinc ion, and the $S_N2$ reaction. The atoms labeled with an asterisk (*) were constrained to remain stationary throughout the geometry optimization. Model C included all parts of Model B (ball-and-tube) and the surrounding active site residues out to 10 Å from the zinc ion (wireframe).

reaction path were re-computed using partial atomic charges in place of the protein atoms in the active site model. As shown in Figure 3A, the use of either Mulliken,[61] Merz–Singh–Kollman[62,63] (MSK), or natural population analysis[64] (NPA) charges gave an energy profile along the reaction path that was nearly identical with the full molecular orbital calculations. This confirmed that the computed barrier suppression at 12.0 Å separation was due to electrostatic interactions. Furthermore, the long-range interactions do not appear to be very sensitive to the particular choice for computing the partial charges.

It is unlikely that an unoccupied coordination site around the zinc ion would remain empty in the native enzyme and that a water molecule would move to fill in this location. We
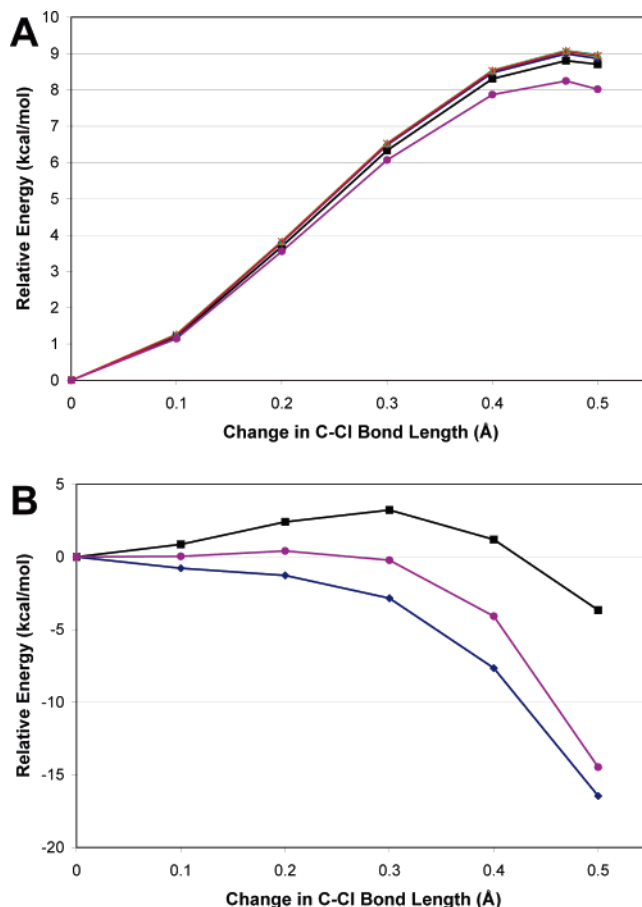


**Figure 3.** (A) Relative energies of points on the $Cl^- + CH_3Cl$ reaction path using Model B with a separation of 12 Å between the central carbon and catalytic zinc ion. The $Cl–CH_3Cl$ ion–molecule complex is at $\Delta R = 0$ Å and the transition state for the reaction occurs at $\Delta R = 0.47$ Å. The data sets correspond to the zinc and amino acid side chains of the active site treated using molecular orbital theory (■, black), Mulliken point charges (◆, blue), MSK point charges (▲, green), and NPA point charges (*, red). Relative energies using molecular orbital theory with a water molecule coordinated to the Zn are also shown (●, purple). (B) Relative energies of points on the $Cl^- + ClCH_3$ reaction path using Models B and C with a separation of 5 Å between the central carbon and catalytic zinc ion. The transition state is at $\Delta R = 0.30$ Å for Model B and $\Delta R = 0.2$ Å for Model C. The data sets correspond to the active site treated using molecular orbital theory (■, black) for Model B, Mulliken point charges (◆, blue) for Model B, and the ONIOM HF/6-31G(d):AM1 method (●, purple) using Model C.

recomputed the relative energies of the $S_N2$ reaction at 12.0 Å separation with a water molecule occupying the empty zinc coordination site. The transition state occurred at approximately the same point on the reaction path and the barrier, 8.3 kcal/mol, was slightly lower than in the absence of the water molecule (see Figure 3A). This helps to validate the exclusion of water from our model at 12.0 Å separation to maintain consistency with the calculations at 5.0 Å separation, since it appears that displacement of water molecules coordinated to the zinc is necessary to accommodate the steric bulk of the iodine as the inhibitor binds to the active site.

Figure 3B illustrates the relative energies on the 5.0 Å reaction path. The transition state occurred much earlier on the reaction path, at a change in $C–Cl_1$ bond length of 0.30 Å compared to 0.47 Å for the 12.0 Å separation, and the barrier was reduced to 3.2 kcal/mol (a barrier suppression of 10.7 kcal/mol or 77% compared to the gas phase reaction). Approximately 0.04 electrons were transferred at the transition state and 0.10 electrons were transferred once the $C–Cl_1$ bond is elongated

by 0.50 Å. Thus charge transfer is not significant until after the barrier has been crossed. To probe the purely electrostatic component of the barrier suppression, single point calculations were carried out on the optimized reaction path with the active site atoms replaced by partial atomic charges. For this model, the transition state barrier for the $S_N2$ displacement reaction disappeared entirely (Figure 3B). This indicated that polarization, present in the full electronic structure calculations, moderated the barrier suppressing effect of the static charge distribution.

*Model C.* While Model B demonstrated that long-range electrostatic interactions significantly influence the $S_N2$ reaction barrier, the lack of protein environment surrounding the active site could lead to inaccurate reaction path energetics due to the concerted effect of long-range electrostatic interactions with the local protein environment. Model C (Figure 2) contained all amino acid residues in CPA that were within a 10 Å radius of the zinc ion in the X-ray structure.[65] This model was divided into two layers and the ONIOM method was used to compute single point energies. The ab initio layer consisted of the model $S_N2$ reaction, the zinc ion, and the fragments of amino acid side chains present in Model B. The semiempirical layer included all the remaining amino acids and residue fragments within 10 Å of the zinc ion and 15 crystallographic water molecules. This scheme allowed for the retention of a much larger fraction of the enzyme in the calculations while still treating the active site with high level ab initio theory. The relative coordinates of the model $S_N2$ reaction at each point on the reaction path were taken from the optimized path for Model B with a Zn−C distance of 5.0 Å.

Calculations of the energy on the reaction path indicated that the transition state occurred even earlier than in Model B (at a C−Cl$_1$ bond elongation of approximately 0.20 Å) and the transition state barrier almost vanished (0.4 kcal/mol, Figure 3B). Comparison with Model B suggested that about $^3/_4$ of the barrier lowering effect in Model C was due to the zinc and its ligands and about $^1/_4$ was due to interaction with the protein environment around the active site. The charge transfer along the reaction path was similar to that observed for Model B (approximately 0.06 electrons transferred at the transition state and 0.26 electrons transferred at 0.50 Å elongation of the C−Cl$_1$ bond). This suggested that interaction with the additional residues present in Model C did not alter the electronic structure of the $S_N2$ transition state; however, it did reduce the barrier by an additional 3 kcal/mol.

**Irreversible Inhibition of CPA by 2-Benzyl-3-iodopropanoate.** The models described above serve as a prelude to the QM/MM calculations on the full CPA enzyme with the actual inhibitor. The electrostatic influence of the active site zinc is moderated by the amino acid side chains that bind the zinc ion. The effect of these ligands cannot simply be replaced by partial charges, since their polarizability plays a significant role. Electrostatic interactions with other residues near the active site also contribute to the lowering of the barrier. All of these factors should be relevant to the interaction of the inhibitor with the enzyme.

The geometry of the pre-reactive complex between CPA and 2-benzyl-3-iodopropanoate has not been determined experimentally, but the geometries of other structurally similar inhibitors bound to CPA have been determined by X-ray crystallography. These structures, particularly 2CTC from the RCSB, served as templates for constructing this complex for use in the QM/MM calculations. Important contacts in the active site of this complex are shown in Figure 4. The structure of the covalently modified product has been determined previously (1BAV in the RCSB[4])
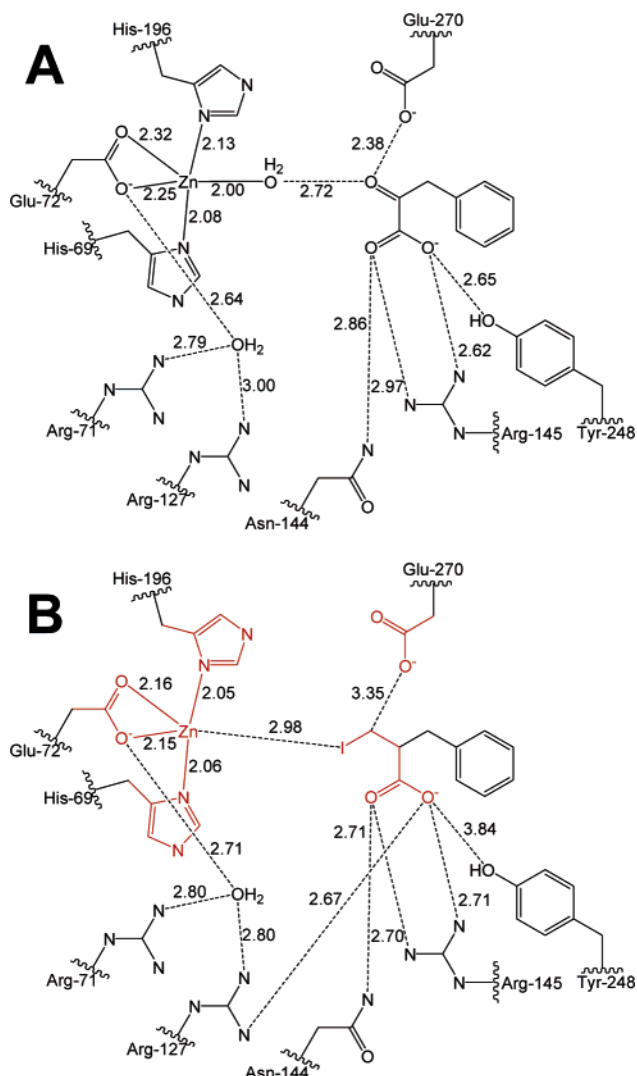


**Figure 4.** (A) Heavy atom bond distances within the 2CTC structure (carboxypeptidase A complexed with L-phenyl lactate) from the RCSB. (B) Heavy atom bond distances within the pre-reactive complex. This was constructed from the 2CTC structure modified to contain the 2-benzyl-3-iodopropanoate inactivator and prepared as described in the Computational Methods section. Atoms shown in red belong to the ab initio layer; all others belong to the molecular mechanics layer.

and can be compared to the end of the reaction path obtained in the QM/MM calculations.

The geometry of the pre-reactive complex was prepared as described in the Computational Methods section, using AMBER to perform MD followed by energy minimization. These MM calculations allow the structure to relax but do not permit any reaction to occur. In the active site, the pentavalent $Zn^{2+}$ ion was coordinated to His-69, Glu-72 (both oxygens were within the coordination sphere of the $Zn^{2+}$ ion), His-196, and a water molecule. The iodopropanoate inactivator was located in the binding pocket of CPA with the iodine oriented toward the $Zn^{2+}$ ion and the carbon that undergoes $S_N2$ displacement was located close to the point of covalent attachment to the carboxylate oxygen of the Glu-270 side chain. Introduction of the phenyl ring of the inactivator within the binding site displaced several crystallographic water molecules observed in the 2CTC X-ray structure. The following atoms were included in the ab initio region of the ONION QM/MM calculations: $Zn^{2+}$, the imidazole ring and β-carbon of His-69 and His-196, the acid group and γ-carbon of Glu-72 and Glu-270, the 2-benzyl-3-iodopropanoate inactivator truncated at the benzyl group, two nearby

**4766**  *J. Phys. Chem. B, Vol. 109, No. 10, 2005*

Cross et al.



**Figure 5.** (A) Heavy atom bond distances within the 1BAV X-ray structure of CPA covalently modified by 2-benzyl-3-iodopropanoate. (B) Heavy atom bond distances within the optimized QM/MM product structure. Atoms shown in red belong to the ab initio layer; all others belong to the molecular mechanics layer.

water molecules, and all hydrogen atoms associated with these molecular fragments. These atoms are shown in red in Figures 4 and 5.

Geometry optimization of the active site region was carried out by allowing all atoms in the ab initio layer, as well as atoms at the QM/MM interface, to move (a total of 73 atoms), while constraining the Cartesian coordinates of the rest of the enzyme to remain fixed. Since the $S_N2$ displacement reaction that resulted in covalent attachment of the inactivator was localized in the binding pocket, this approximation was justified. As well, this enabled the optimization to proceed much more rapidly than if the entire enzyme were optimized by reducing numerical noise due to protein conformational changes that could have occurred at a distance from the active site.

The MD simulation and subsequent energy minimization of the pre-reactive protein–ligand complex during protein preparation maintained several structural motifs within the binding site of CPA present in the X-ray geometry of the parent structure, 2CTC. The Arg-127 side chain extended further into the binding pocket for both the 2CTC and the prepared complex containing the 2-benzyl-3-iodopropanoate inactivator (Figure 4B) than in the noncomplexed 2CTB structure. The side chain of Tyr-248 also remained in the "down position" rather than in the orientation observed in the 2CTB structure with no bound
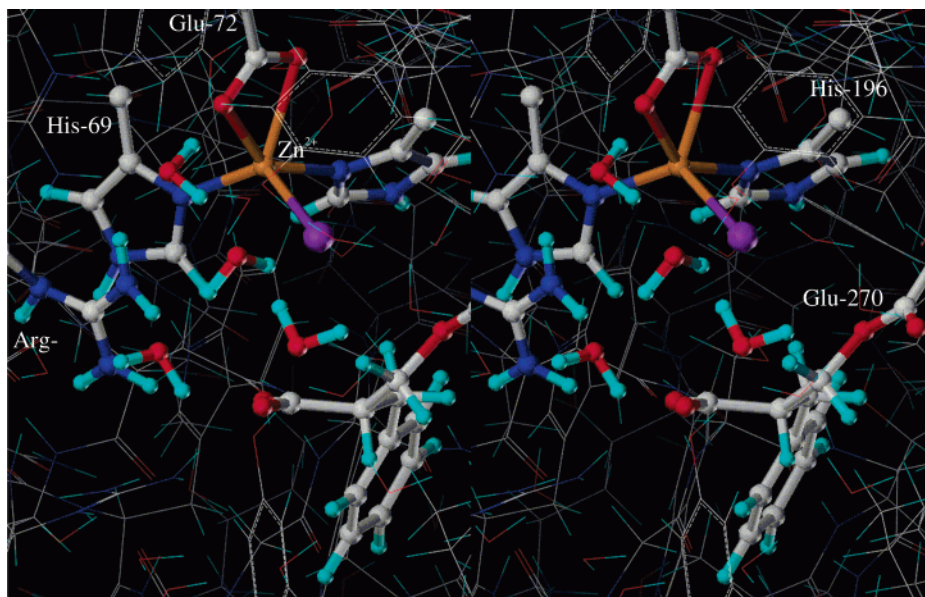
substrate.[66,67] The $N-C_\alpha-C_\beta-C_\gamma$ dihedral angle of Tyr-248 was 34° in the 2CTC structure and 36° in the pre-reactive complex compared to 162° for the 2CTB structure. This conformation of Tyr-248 is found in many CPA X-ray structures, including the 2CTC structure complexed with L-phenyl lactate and the 1BAV structure with the covalently attached inactivator. In the native enzyme with the natural substrate, this geometrical restructuring allows the hydroxyl group of Tyr-248 to make a hydrogen bond with the terminal carboxylate of the substrate.[66,67] The formation of a hydrogen bond was also possible between the hydroxyl group of the phenol and the carboxylate group of the inactivator (2.65 Å for 2CTC and 3.84 Å for the pre-reactive complex) with this Tyr-248 conformation. Additionally, the steric bulk of the halide group belonging to the inactivator caused the Zn-bound water molecule that appears in the 2CTC structure to move out of the coordination sphere of the $Zn^{2+}$ ion. Formation of the pre-reactive complex placed the iodine atom very close to the $Zn^{2+}$ ion (2.98 Å), completely blocking the catalytic cation from the solvent.

The geometry of the MM minimized pre-reactive complex (Figure 4B) was used as the input structure for QM/MM optimization. Over the course of the optimization, a carboxylate oxygen atom belonging to Glu-270 displaced the iodine of the inactivator and the displaced iodide became bound to the $Zn^{2+}$ ion, resulting in formation of the covalently modified inactivation product (Figures 5 and 6). Since the geometry optimization algorithm always steps in a downhill direction, this suggests there is little or no barrier for the reaction. Several points along the reaction path were computed by constraining the carbon–iodine distance and optimizing the remaining coordinates. The energy decreased monotonically, confirming that the displacement of the iodide and subsequent rearrangement of the active site is a barrierless process at the present level of theory. In essence, once the inactivator is in the CPA active site there is no enthalpic barrier for the covalent modification of Glu-270.

The geometric details of the active site in the QM/MM optimized product structure are outlined in Figure 5B and are shown in stereo in Figure 6. The $Zn^{2+}$ ion remained coordinated to His-69, Glu-72, and His-196, with iodine in place of the water molecule present in the X-ray structures (Zn–I bond length of 2.72 Å). The CPA side chains bound to the $Zn^{2+}$ ion remained relatively unchanged, with Zn–N bond lengths of 2.11 and 2.08 Å to His-69 and His-196, respectively, and Zn–O bond lengths of 2.04 and 2.45 Å to Glu-72. A water molecule remained hydrogen bonded to the Zn-bound iodine at a distance of 3.21 Å, and became part of an extended hydrogen bond network between several local water molecules in the binding site and the Arg-71, Glu-72, and Arg-127 side chains. Arg-127 was also oriented properly to form a weak salt bridge between its guanidinium moiety and one oxygen atom belonging to the carboxylate group of the covalently attached inactivator. However, a minor conformational change in the side chain orientation of Arg-145 allowed the positively charged guanidinium group to form a stronger salt bridge with the second oxygen atom in the inhibitor's carboxylate group (2.96 Å).[67] Additionally, the covalent bond between the 2-benzyl-3-iodopropanoate inactivator and Glu-270 was completely formed (C–O bond length of 1.47 Å compared to 1.43 Å in the 1BAV X-ray structure of the covalently attached inactivator[4]) with the iodide ion located 3.53 Å from the central carbon that was the site of the $S_N2$ reaction. This iodide ion was not present in the X-ray structure and a water molecule occupied the final coordination site around the $Zn^{2+}$ ion.

**Figure 6.** Stereoview of the QM/MM optimized reaction product.

Most of the geometrical features observed in the CPA active site region after both the protein preparation and the QM/MM optimization steps were not unexpected, and remained consistent with experimental X-ray structures.[4,67] However, covalent attachment of the inactivator to the carboxylate group of Glu-270 induced a significant change in the $C_\beta-C_\gamma$ torsion of the side chain in the QM/MM structure when compared to the corresponding X-ray structures of the covalently inactivated protein[4] and the noncovalently modified protein. In the X-ray structure of unmodified CPA, the Glu-270 side chain extended toward the catalytic $Zn^{2+}$ ion and formed a hydrogen bond with a Zn-bound water molecule (2.66 Å), with a $C_\alpha-C_\beta-C_\gamma-C_\delta$ dihedral angle of 279°. The X-ray structure of the covalently modified protein was very similar to this, with the carbonyl oxygen of the ester group from the covalently modified Glu-270 side chain pointing toward a zinc-bound water molecule (3.01 Å) and a $C_\alpha-C_\beta-C_\gamma-C_\delta$ dihedral angle of 286°. In the QM/MM optimized structure, this dihedral angle changed to 188°, which caused a conformational shift of the covalently modified Glu-270 ester group away from the catalytic site. The presence of the water molecule in the zinc coordination sphere of the X-ray structure could account for this difference, since this allowed an opportunity for hydrogen bonding with the newly formed ester linkage, possibly mediated by an additional water molecule not seen in the X-ray. The iodide ion that appeared in the same position coordinated to zinc in the QM/MM product structure prevented this hydrogen bonding interaction from taking place, and a torsional shift was required to satisfy the hydrogen bonding potential of the ester linkage with another nearby hydrogen bond donor.

This torsional rearrangement of the ester linkage between enzyme and inhibitor positioned the carbonyl group such that it could form a hydrogen bond with Ser-199 after some movement of its side chain, which, while not part of the QM region, was allowed to relax during the QM/MM optimization. In the X-ray structure of unmodified CPA, the hydroxyl group of Ser-199 is hydrogen bonded to the backbone carbonyl group of Tyr-198 (2.66 Å) and lies 5.63 Å from the carboxylate oxygen atoms of the Glu-270 side chain. Over the course of the optimization, the α-carbon and hydroxyl oxygen atoms of Ser-199 moved toward the Glu-270 residue by 1.00 and 2.74 Å, respectively, which resulted in the loss of the hydrogen bond

to Tyr-198 and the formation of a hydrogen bond between the Ser-199 hydroxyl group and the carbonyl oxygen atom of the modified Glu-270 side chain ester (3.30 Å). Although similar torsional changes were apparent in the X-ray structure of the covalently modified enzyme, the location of the Glu-270 side chain prevented hydrogen bonding with the Ser-199 side chain.

## Conclusions

In this study, we have examined inactivation of CPA by 2-benzyl-3-iodopropanoate. The zinc ion in the active site promotes an $S_N2$ reaction between Glu-270 and the alkyl halide bond of the inhibitor to form a covalent bond that irreversibly inactivates the enzyme. We have used a series of simple models of the active site and a generic $S_N2$ reaction to probe the nature of these interactions. Using a bare zinc ion (Model A) was too severe an approximation, but when the side chains coordinated to the zinc ion were included (Model B), the effects on the $S_N2$ barrier were more sensible. At large separation the interaction is entirely electrostatic, but at shorter distances polarization of the ligands starts to play a role. Hence, both the zinc ion and its ligands must be treated quantum mechanically. When all the residues within 10 Å of the active site zinc were included in the ONIOM MO/MO calculations, the barrier was reduced to a fraction of a kcal/mol. About $^3/_4$ of the barrier suppression is due to the zinc ion and its ligands, and the remainder is due to the residues surrounding the active site. The QM/MM calculations using the real inhibitor and the fully solvated enzyme revealed a barrierless reaction path for inactivation of CPA by 2-benzyl-3-iodopropanoate once the pre-reactive complex between the protein and ligand was formed. This is consistent with the large rate enhancement observed for the $S_N2$ reaction between the enzyme and the inhibitor,[3] as well as our previous inability to crystallize the pre-reactive complex due to rapid enzyme modification.[4]

The catalytic mechanism of CPA, and other zinc-dependent proteases, has been scrutinized over the years. There are two major proposals for the mechanism in the literature, as well as a relatively new proposal that contains elements of both mechanisms,[14] all of which rely on zinc chemistry to drive the process. The active site glutamate, Glu-270 of CPA, is conserved in all zinc proteases and it is believed to serve the role of the

Cross et al.

general base in the "promoted-water" mechanism suggested for these enzymes.[67] In the alternative mechanism for catalysis by CPA, it has been proposed that this glutamate is involved in the formation of a mixed anhydride with the substrate prior to hydrolysis of the intermediate.[68−70] In either case, the chemistry at the glutamate site is indispensable for the catalytic processes of zinc proteases, and its covalent modification by our inactivator leads to irreversible loss of activity.

**Supporting Information Available:** Tables of geometries and energies of the reported structures, relative energies for Models B and C, and RESP charges for the 2-benzyl-3-iodopropanoate inactivator. This material is available free of charge via the Internet at http://pubs.acs.org.

## References and Notes

(1) Kim, D. H.; Mobashery, S. Mechanism-Based Inhibition of Metalloproteinases. *Frontiers Med. Chem.* **2004**, *8*, 959−965.

(2) Ghosh, S. S.; Wu, Y.-Q.; Mobashery, S. *J. Biol. Chem.* **1991**, *266*, 8759−8764. Wu, Y. Q.; Mobashery, S. *J. Med. Chem.* **1991**, *34*, 1914−1916.

(3) Tanaka, Y.; Grapsas, I.; Dakoji, S.; Cho, Y. J.; Mobashery, S. *J. Am. Chem. Soc.* **1994**, *116*, 7475−7480.

(4) Massova, I.; Martin, P.; Mel, S. D.; Tanaka, Y.; Edwards, B.; Mobashery, S. *J. Am. Chem. Soc.* **1996**, *118*, 12479−12480.

(5) Bloch, K. E. *J. Protein Chem.* **1986**, *5*, 69.

(6) Liang, J.-Y.; Lipscomb, W. N. *Biochemistry* **1987**, *26*, 5293−5301.

(7) Jacob, O.; Cardenas, R.; Tapia, O. *J. Am. Chem. Soc.* **1990**, *112*, 8692−8705.

(8) Solà, M.; Lledós, A.; Bertrán, J. *Inorg. Chem.* **1991**, *30*, 2523−2527.

(9) Jacob, O.; Tapia, O. *Int. J. Quantum Chem.* **1992**, *42*, 1271−1289.

(10) Merz, K. M., Jr.; Hoffman, R.; Dewar, M. J. S. *J. Am. Chem. Soc.* **1989**, *111*, 5636−5649.

(11) Alex, A.; Clark, T. *J. Comput. Chem.* **1992**, *13*, 704−717.

(12) Onciul, A. R. v.; Clark, T. *J. Comput. Chem.* **1993**, *14*, 392−400.

(13) Torrent, M.; Vreven, T.; Musaev, D. G.; Morokuma, K.; Farkas, O.; Schlegel, H. B. *J. Am. Chem. Soc.* **2002**, *124*, 192−193.

(14) Pelmenschikov, V.; Blomberg, M. R. A.; Siegbahn, P. E. M. *J. Biol. Inorg. Chem.* **2002**, *7*, 284−298.

(15) Morihara, K.; Tsuzuky, H. *Eur. J. Biochem.* **1970**, *15*, 374.

(16) Gao, J. In *Reviews in Computational Chemistry*; Lipkowitz, K. B., Boyd, D. B., Eds.; VCH: New York, 1996; Vol. 7, pp 119−185.

(17) Froese, R. D. J.; Morokuma, K. In *Encyclopedia of Computational Chemistry*; Schleyer, P. v. R.; Allinger, N. L.; Kollman, P. A.; Clark, T.; Schaefer, H. F., III; Gasteiger, J., Schreiner, P. R., Eds.; Wiley: Chichester, 1998; Vol. 2, pp 1244−1257.

(18) Tomasi, J.; Pomeli, C. S. In *Encyclopedia of Computational Chemistry*; Schleyer, P. v. R.; Allinger, N. L., Kollman, P. A., Clark, T.; Schaefer, H. F., III, Gasteiger, J., Schreiner, P. R., Eds.; Wiley: Chichester, UK, 1998; Vol. 4, pp 2343−2350.

(19) Ruiz-López, M. F.; Rivail, J. L. In *Encyclopedia of Computational Chemistry*; Schleyer, P. v. R.; Allinger, N. L., Kollman, P. A., Clark, T.; Schaefer, H. F., III, Gasteiger, J., Schreiner, P. R., Eds.; Wiley: Chichester, UK, 1998; Vol. 1, pp 437−448.

(20) Monard, G.; Merz, K. M. *Acc. Chem. Res.* **1999**, *32*, 904−911.

(21) Dinner, A. R.; Blackburn, G. M.; Karplus, M. *Nature* **2001**, *413*, 752−755.

(22) Zhang, Y.; Kua, J.; McCammon, J. A. *J. Am. Chem. Soc.* **2002**, *124*, 10572−10577.

(23) Castillo, R.; Silla, E.; Tunon, I. *J. Am. Chem. Soc.* **2002**, *124*, 1809−1816.

(24) Thomas, A.; Field, M. J. *J. Am. Chem. Soc.* **2002**, *124*, 12432−12438.

(25) Li, J.; Cross, J. B.; Vreven, T.; Meroueh, S. O.; Mobashery, S.; Schlegel, H. B. Submitted for publicaiton.

(26) Warshel, A. *J. Biol. Chem.* **1998**, *273*, 27035−27038.

(27) Villà, J.; Štrajbl, M.; Glennon, T. M.; Sham, Y. Y.; Chu, Z. T.; Warshel, A. *Proc. Natl. Acad. Sci. U.S.A.* **2000**, *97*, 11899−11904.

(28) Andrés, J. L.; Lledós, A.; Duran, M.; Bertrán, J. *Chem. Phys. Lett.* **1988**, *153*, 82−86.

(29) Carbonell, E.; Duran, M.; Lledós, A.; Bertrán, J. *J. Phys. Chem.* **1991**, *95*, 179−183.

(30) Maseras, F.; Morokuma, K. *J. Comput. Chem.* **1995**, *16*, 1170−1179.

(31) Dapprich, S.; Komaromi, I.; Byun, K. S.; Morokuma, K.; Frisch, M. J. *J. Mol. Struct. THEOCHEM* **1999**, *462*, 1−21.

(32) Vreven, T.; Morokuma, K. *Theor. Chem. Acc.* **2003**, *109*, 125−132.

(33) Frisch, M. J.; Trucks, G. W.; Schlegel, H. B.; Scuseria, G. E.; Robb, M. A.; Cheeseman, J. R.; Montgomery, J. A., Jr.; Vreven, T.; Kudin, K. N.; Burant, J. C.; Millam, J. M.; Iyengar, S. S.; Tomasi, J.; Barone, V.; Mennucci, B.; Cossi, M.; Scalmani, G.; Rega, N.; Petersson, G. A.; Nakatsuji, H.; Hada, M.; Ehara, M.; Toyota, K.; Fukuda, R.; Hasegawa, J.; Ishida, M.; Nakajima, T.; Honda, Y.; Kitao, O.; Nakai, H.; Klene, M.; Li, X.; Knox, J. E.; Hratchian, H. P.; Cross, J. B.; Adamo, C.; Jaramillo, J.; Gomperts, R.; Stratmann, R. E.; Yazyev, O.; Austin, A. J.; Cammi, R.; Pomelli, C.; Ochterski, J. W.; Ayala, P. Y.; Morokuma, K.; Voth, G. A.; Salvador, P.; Dannenberg, J. J.; Zakrzewski, V. G.; Dapprich, S.; Daniels, A. D.; Strain, M. C.; Farkas, O.; Malick, D. K.; Rabuck, A. D.; Raghavachari, K.; Foresman, J. B.; Ortiz, J. V.; Cui, Q.; Baboul, A. G.; Clifford, S.; Cioslowski, J.; Stefanov, B. B.; Liu, G.; Liashenko, A.; Piskorz, P.; Komaromi, I.; Martin, R. L.; Fox, D. J.; Keith, T.; Al-Laham, M. A.; Peng, C. Y.; Nanayakkara, A.; Challacombe, M.; Gill, P. M. W.; Johnson, B.; Chen, W.; Wong, M. W.; Gonzalez, C.; Pople, J. A. *GAUSSIAN 03*, Revision A.1; Gaussian, Inc.: Pittsburgh, PA, 2003.

(34) Roothaan, C. C. J. *Rev. Mod. Phys.* **1951**, *23*, 69−89. Hall, G. G. *Proc. R. Soc. (London)* **1951**, *A205*, 541−552.

(35) Ditchfield, R.; Hehre, W. J.; Pople, J. A. *J. Chem. Phys.* **1971**, *54*, 724−728.

(36) Hariharan, P. C.; Pople, J. A. *Theor. Chim. Acta* **1973**, *28*, 213−222.

(37) Chandrasekhar, J.; Smith, S. F.; Jorgensen, W. L. *J. Am. Chem. Soc.* **1985**, *107*, 154−163.

(38) Wachters, A. J. H. *J. Chem. Phys.* **1970**, *52*, 1033−1036.

(39) Hay, P. J. *J. Chem. Phys.* **1977**, *66*, 4377−4384.

(40) Raghavachari, K.; Trucks, G. W. *J. Chem. Phys.* **1989**, *91*, 1062−1065.

(41) Dewar, M. J. S.; Zoebisch, E. G.; Healy, E. F. *J. Am. Chem. Soc.* **1985**, *107*, 3902−3909.

(42) Vreven, T.; Morokuma, K.; Farkas, O.; Schlegel, H. B.; Frisch, M. J. *J. Comput. Chem.* **2003**, *24*, 760−769.

(43) Kollman, P. A.; Dixon, R.; Cornell, W. D.; Fox, T.; Chipot, C.; Pohorille, A. In *Computer Simulations of Biomolecular Systems*; Wilkinson, A., Weiner, P., van Gunsteren, W., Eds.; Elsevier: New York, 1997; Vol. 3, pp 83−96.

(44) *SYBYL 6.7*; Tripos Inc.: 1699 South Hanley Rd., St. Louis, MO, 63144.

(45) Case, D. A.; Pearlman, D. A.; Caldwell, J. W.; Cheatham, T. E., III; Ross, W. S.; Simmerling, C. L.; Darden, T. A.; Merz, K. M.; Stanton, R. V.; Cheng, A. L.; Vincent, J. J.; Crowley, M.; Tsui, V.; Radmer, R. J.; Duan, Y.; Pitera, J.; Massova, I.; Seibel, G. L.; Singh, U. C.; Weiner, P. K.; Kollman, P. A. *AMBER 6*; University of California: San Francisco, CA, 1999.

(46) Wang, J.; Cieplak, P.; Kollman, P. A. *J. Comput. Chem.* **2000**, *21*, 1049−1074.

(47) Bayly, C. I.; Cieplak, P.; Cornell, W. D.; Kollman, P. A. *J. Chem. Phys.* **1993**, *97*, 10269−10280.

(48) Yang, P. F.; Yang, G. K. *J. Am. Chem. Soc.* **1992**, *114*, 6937−6938.

(49) Gomes-Carneiro, T. M.; Jackson, R. D.; Downing, J. H.; Orpen, A. G.; Pringle, P. G. *J. Chem. Soc., Chem. Commun.* **1991**, 317.

(50) Kulawiec, R. J.; Faller, J. W.; Crabtree, R. H. *Organometallics* **1990**, *9*, 745−755.

(51) Colsman, M. R.; Newbound, T. D.; Marshall, L. J.; Noirot, M. D.; Miller, M. M.; Wulfsberg, G. P.; Frye, J. S.; Anderson, O. P.; Strauss, S. H. *J. Am. Chem. Soc.* **1990**, *112*, 2349−2362.

(52) Brown, M.; Waters, J. M. *J. Am. Chem. Soc.* **1990**, *112*, 2442−2443.

(53) Winter, C. H.; Veal, W. R.; Garner, C. M.; Arif, A. M.; Gladysz, J. A. *J. Am. Chem. Soc.* **1989**, *111*, 4766−4776.

(54) Kulawiec, R. J.; Crabtree, R. H. *Coord. Chem. Rev.* **1990**, *99*, 89−115.

(55) Mitchell, D. J.; Schlegel, H. B.; Shaik, S. S.; Wolfe, S. *Can. J. Chem.* **1985**, *63*, 1642−1648.

(56) Luke, B. T.; Loew, G. H.; McLean, A. D. *Int. J. Quantum Chem.* **1986**, *29*, 883−896.

(57) Tucker, S. C.; Truhlar, D. G. *J. Phys. Chem.* **1989**, *93*, 8138−8142.

(58) Mann, D. J.; Hase, W. L. *J. Phys. Chem. A* **1998**, *102*, 6208−6214.

(59) Li, G.; Hase, W. L. *J. Am. Chem. Soc.* **1999**, *121*, 7124−7129.

(60) Shaik, S. S.; Pross, A. *J. Am. Chem. Soc.* **1982**, *104*, 2708−2719.

(61) Mulliken, R. S. *J. Chem. Phys.* **1955**, *23*, 1833−1840.

(62) Singh, U. C.; Kollman, P. A. *J. Comput. Chem.* **1984**, *5*, 129−145.

(63) Besler, B. H.; Merz, K. M., Jr.; Kollman, P. A. *J. Comput. Chem.* **1990**, *11*, 431−439.

(64) Reed, A. E.; Curtiss, L. A.; Weinhold, F. *Chem. Rev.* **1988**, *88*, 899−926.

(65) This includes the following residues: Asp-65, Leu-66, Gly-67, Ile-68, His-69, Ser-70, Arg-71, Glu-72, Arg-127, Asp-142, Ala-143, the peptide backbone of Asn-144, the side chain of Arg-145, Ser-194, Ile-195, His-196, Ser-197, Ser-199, Thr-268, the peptide backbone of Phe-269, Glu-270, Leu-271, and the side chain of Phe-279.

(66) Christianson, D. W.; Lipscomb, W. N. *Proc. Natl. Acad. Sci. U.S.A.* **1986**, *83*, 7568−7572.

(67) Christianson, D. W.; Lipscomb, W. N. *Acc. Chem. Res.* **1989**, *22*, 62−69.

(68) Makinen, M. W.; Kuo, L.; Dymowski, J. J.; Jaffer, S. *J. Biol. Chem.* **1979**, *254*, 356−366.

(69) Makinen, M. W.; Wells, G. B.; Kang, S. O. *Adv. Inorg. Biochem.* **1984**, *6*, 1−69.

(70) Suh, J. *Bioorg. Chem.* **1990**, *18*, 345−360.